Accepted Manuscript

Vanadium oxide nanorings: facile synthesis, formation mechanism and electrochemical properties[¥][≠]

G. Nagaraju[a,b][*] nagarajugn@rediffmail.com, S. Ashoka[c], R. Manjunatha[d], S. Srinivasan[d], J. Livage[e], G. T. Chandrappa[b]

[a]Department of Chemistry, Siddaganga Institute of Technology, Tumakuru, India.

[b]Department of Chemistry, Central College Campus, Bangalore University, Bangalore, India.

[c]Department of Chemistry, Dayananda Sagar Univeristy, Bangalore, India.

[d]Department of Inorganic and Physical Chemistry, Indian Institute of Science, Bangalore, India.

[e]Laboratoire Chimie de la Matière Condensée, Collège de France, Place Marcelin Berthelot, Paris cedex 05, France.

[*]Corresponding author.

[¥]Electronic supplementary information's (ESI) are available: SEM images for the variations of experimental parameters and charge-discharge profile.

[≠]Dedicated to 109th Birthday (born April1, 1907) of Dr. Sree Sree Sree Shivakumara Mahaswamiji, Siddaganga Matta, Tumakuru, Karnataka, India.

Graphical Abstract
fx1
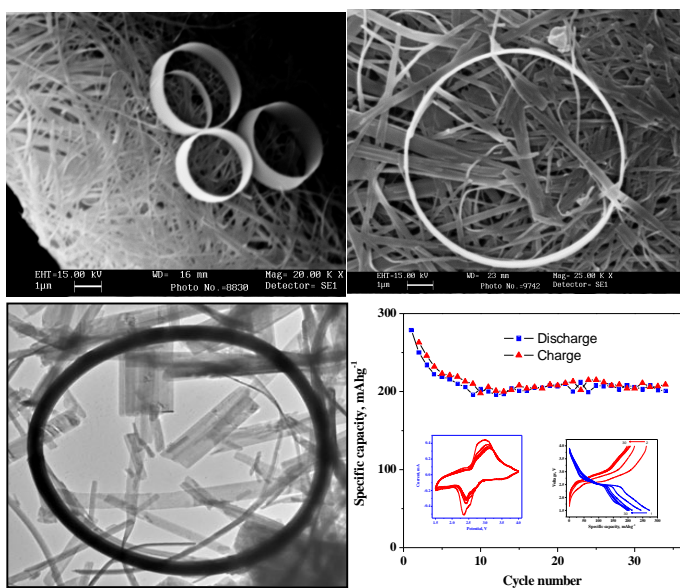
Highlights

1. Synthesis via hydrothermal method without using any surfactant in acidic medium.

2. Rings were formed in a wide range of temperature from 100-180 °C for 1-3 days.

3. The cyclability of Li ion battery of the material is relatively good.

4. Because of mixed phase it is not possible to compare with pure V_2O_5 battery.

5. A probable reaction mechanism for the formation of V_2O_5 nanorings is proposed.

ABSTRACT

This paper describes the hydrothermal synthesis of vanadium oxide nanorings and nanobelts from aqueous precursors without using any template. These nanorings are formed via the acidification of sodium metavanadate solution. A simple ion intercalation/de-intercalation process occurs under mild hydrothermal conditions leading to the self-rolling of exfoliated vanadium oxide nanobelts. The structure and morphology of the products are characterized by XRD, SEM, TEM and charge-discharge measurement. XRD pattern reveals that the products consist of V_2O_5 nanorings and $Na_{0.3}V_2O_5$ nanobelts evidenced by SEAD pattern and EDS. Highly magnified TEM images exhibit nanorings made of nanoribbons of width about 300 nm and thickness of about 60 nm. Electrochemical analyses revealed that the V_2O_5 nanorings/nanobelts delivers an initial lithium-ion intercalation capacity of 280 mAh g^{-1} and reaches a stabilized capacity of 200 mAh g^{-1} at a current density of 100 mA g^{-1}.

*Keywords: A. N*anostructures; A. Layered compound; B. Chemical synthesis; B. Intercalation reactions; C. X-ray diffraction; C: Electrochemical measurements; D: Energy storage.

1. Introduction

1-D nanostructured transition metal oxides exhibits a unique class of materials because of their redox activity, which is connected with outstanding electrochemical and catalytic properties. Among transition metal oxides, layered vanadium pentoxide (Eg = 2.8 eV) and its compounds allow a wide range of practical applications such as lithium batteries [1-6], catalysis, [7,8], electro-chromic devices [9], supercapacitors [10], actuators [11], sensors [12] etc, due to their outstanding structural flexibility combined with chemical and physical properties.

V_2O_5 is a typical intercalation compound with a layered crystal structure that can be reversibly intercalated and de-intercalated between the layers has been extensively studied as a cathode material for rechargeable lithium batteries because of its low cost, abundance, easy synthesis and high energy density [13]. However, the development of rechargeable lithium batteries with V_2O_5 as a cathode material has been limited due to its poor structural stability, low electronic and ionic conductivity, and slow electrochemical kinetics [14,15]. It is well known that the structure and morphology of V_2O_5 can strongly influence its electrochemical performance. In recent years, a lot of research has been focused on the synthesis and fabrication of 1-D nanostructured V_2O_5. It has been demonstrated that V_2O_5 nanorods, nanotubes, nanowires, nanoribbons, etc, are regarded as promising active lithium intercalation cathode materials because they provide shorter path lengths for both electronic and Li ionic transport [16].

V_2O_5. nH_2O and cation intercalated V_2O_5 [$M_{0.3}V_2O_5.nH_2O$ (M = Li^+, Na^+)] have been extensively studied for their electrochemical properties. They consist of V_2O_5 bilayers whose interlayer space is occupied by water molecules (V_2O_5. nH_2O) and cations ($Na_{0.3}V_2O_5$. nH_2O). In the case of $Na_{0.3}V_2O_5$. nH_2O, the structural anisotropy of the particles was shown to induce a

5

better electrochemical response, compared to the analogous compound synthesized by solid state reactions [17,18].

Although various methods are available for the synthesis of low dimensional V_2O_5 nanostructured electrode materials [19-25], many of them suffer from the limits of high temperatures, special equipment's and/or special experimental conditions. The hydrothermal synthesis remains interesting because it is a powerful tool to transform transition metal oxides into high quality nanostructures and nanostructured vanadium oxides in different morphologies besides lower temperature involved in the cost effective environmentally benign process.

A common preparative procedure for nanostructured vanadium oxide materials from molecular clusters to 1-D and 2-D layered compounds involves the hydrothermal treatment of a vanadium precursor (Ex. NH_4VO_3, Vanadium alkoxides, V_2O_5 or $VOSO_4$). Nanotubes are obtained via a self-rolling process while amazing morphologies such as nanospheres, nanoflowers and even nanourchins are formed via the self-assembling of nanoparticles [26]. Control over the nucleation and growth may be crucial in the tailoring of the size, shape, surface structure and consequently to the final properties of the resultant VOx materials.

Increasing attention is being nowadays paid to ring [27-32] like nanomaterials because of their size, special morphology-related properties and potential nanoscale applications [31]. This paper reports on the synthesis and the electrochemical performance of V_2O_5 nanorings and $Na_{0.3}V_2O_5$ nanoribbons obtained under hydrothermal conditions. The mechanism for the formation of nanorings is also discussed.

2. Experimental

Hydrothermal process was carried out like our previous report to synthesis Ammonium vanadate nanorings or Cadmium carbonate nanorings [33, 34]. 0.27 g $NaVO_3$ was dissolved in 20 mL

6

distilled water taken in a 30 mL capacity Teflon tube. Two drops of HCl (pH≈ 3-4) was added to it to maintain acidic medium and stirred for 10 min. The resultant wine-red solution was subjected to hydrothermal treatment from 100 °C to 180 °C for 1-3 days. The reddish-brown non-adherent spongy-like bulky material was collected and washed with distilled water and absolute alcohol several times before being dried in air.

2.1 Characterizations

Powder X-ray diffraction data were recorded on Philips X'pert PRO X-ray diffractometer with graphite monochromatized Cu-Kα (1.5418 Å) radiation. The Fourier transform infrared spectrum (FTIR) of the sample was collected using Bruker Alpha-P spectrometer. The absorption spectrum of the sample was measured on a Perkin Elmer Lambda-750 UV-Visible spectrometer. The morphology of the product was examined by JEOL-JSM–6490 LV scanning electron microscope (SEM) and CM12 Philips transmission electron microscope (TEM) equipped with energy dispersive X-ray spectrometer (EDS). The BET-surface area measurements were carried out using QUADRASORB SI quantachrome instrument.

The electrochemical properties of the V_2O_5 nanorings/nanoribbons were tested in Swagelok cells assembled in an argon filled glove box (Jacomex). The cathode electrodes were made by mixing 70 wt.% active material (V_2O_5 nanorings/ribbons), 20 wt.% conductive material (acetylene black) and 10 wt.% binder [poly(vinylene difluoride, PVDF]. The slurry prepared using 1-methyl-2-pyrrolidone (NMP) as a solvent was coated on Al foil as a current collector, finally dried in the oven at 120 ^{0}C for one day. Lithium metal was used as the counter and reference electrodes. The electrolyte was 1 M $LiPF_6$ in ethylene carbonate (EC) and dimethylene carbonate (DMC) (1:1 v/v). Cyclic voltammetry (CV) measurements are performed using CHI 660C (CH Instrument Electrochemical workstation) between 1.5 - 4.0 V versus Li^+/Li at a scan

rate of 0.5 mVs^{-1}. Galvanostatic discharge/charge measurements were performed on an Arbin BT-2000 battery tester between 1.5 - 4.0 V versus Li$^+$/Li.

3. Results and Discussion

3.1 Structural characterization

The XRD patterns (Fig. 1) exhibit the phases and purities of the samples V_2O_5 nanorings (JCPDS 85-2422) and $Na_{0.3}V_2O_5$ nanoribbons/ribbons (JCPDS 75-0544). The composition of V_2O_5 nanorings and $Na_{0.3}V_2O_5$ nanoribbons were well evidenced by EDS analyses (Fig. 2). EDS spectrum taken on the nanorings shows the absence of sodium clearly indicates that nanorings are made up of only V and O.

Fig. 3a shows the FTIR spectrum of the V_2O_5 nanorings/nanoribbons. The peak at 1002 cm^{-1} is characteristic of the stretching vibration of the terminal vanadyl V=O. The absorption bands at 826 and 534 cm^{-1} can be attributed to the asymmetric and symmetric stretching vibrations of V-O-V bonds respectively. The IR spectrum of the $Na_{0.3}V_2O_5$ is quite similar except for the bands corresponding to the stretching vibration of V=O. Indeed, in addition to the vibration at 1002 cm^{-1} a shoulder at 965 cm^{-1}, corresponding to a weaker V=O vibration is evidenced and its intensity increases with initial pH values [18, 35]. To evaluate the optical properties of the V_2O_5 nanorings/nanoribbons, UV–Vis spectrum was recorded from 200-800 nm and is shown in Fig. 3b V_2O_5 nanorings/nanoribbons shows maximum absorbance at 462 nm is blue-shifted compared to that of bulk V_2O_5 powders (470 nm). The origin of the blue shift in the absorption band is suggested to be the contribution of a quantum size effect in V_2O_5 nanorings/nanoribbons [32].

SEM is used as important technique to identify the morphological architecture of the samples prepared under hydrothermal method from 100-180 °C for 1-3 days. Selective images of SEM

with interesting morphologies have been taken into consideration. Nanorings obtained at 100 °C and 110 °C for 3 days (Fig. 4) were made of ribbons that have typical diameters of 3-4 µm and 0.5-1 µm wide shells with a thickness of about 60-80 nm. Samples obtained at 130 °C for 1 day (Fig. 5a,) consist of nanorings of various sizes made of nanoribbons and nanoribbons. Curving of nanoribbons/ribbons takes place extensively under this condition. SEM images of the product prepared at 130 °C for 2 days (Fig. 5b-c, Fig. S1) show that the dispersed nanorings lay on randomly folded nanocarpets made of nanoribbons only. Highly magnified SEM images exhibit nanorings made of nanoribbons of width 200-300 nm and thickness of about 60 nm. With an increase in temperature to 150 °C for 1 day, concentric nanorings resembling tires of automobiles (Fig. 5d) are formed. As the reaction time was an increase from 2 to 3 days (Fig. S2), nest structure gradually decreases. At 130 °C (Fig. 5b-c) and 150 °C (Fig. 5e-f) for 2 days, a significant amount of nanoribbons were curved into perfect circular shape, which was not found for nanoribbons or nanowires of the VO_x family. The synthesized samples are composed of many freestanding nanorings at a significant percentage ($\sim$ 40 to 50%) of the yield and $\sim$70% of the reproducibility from run to run.

Experiments were carried out to know the effect of temperature, nature of the acid, concentration of the precursor, nature of the precursor, etc. on the morphology of the product obtained. Nanorings were not formed for H_2SO_4 and HNO_3 at 130 °C for 2 days. Nanorings are not observed when the concentration of the precursor is halved and only few nanorings were observed when the concentration is doubled (Fig. S3b). Fig. S4 and Fig. S5 shows the morphology of the product prepared at 160 °C and 180 °C for 1-3 days. It shows that at higher temperature, number of rings formed was decreases. Changing the precursor from sodium

9

vanadate to ammonium vanadate, no rings were observed at all experimental conditions (Fig. S6), which clearly indicates that sodium, was necessary for the formation of V_2O_5 nanorings.

Fig. 6 shows the TEM image and SAED pattern of nanorings/nanoribbons prepared at 110 °C for 3 days and 150 °C for 2 days. The sample (Fig. 6a,b) was composed mainly of nanoribbons and nanorings. The thickness of the nanorings was found to be about 200 nm and nanoribbons was 100-200nm. The HRTEM image (Fig. 6b inset) recorded on the quadrate area of nanorings shows clearly the resolved inter planar distances *(d= 0.71 nm)*, which determine the *(101)* growth direction of the nanorings. The clear diffraction circles shown in the SAED pattern (Fig. 6e) can be well attributed to the diffraction of *(202), (111), (211), (401)* and *(502)* planes of V_2O_5 nanoring from inside to outside. The lattice fringe with a spacing of 0.71 nm in HRTEM image is in agreement with the 'd' value (0.706 nm) of orthorhombic V_2O_5. TEM images of the sample prepared at 150 °C for 2 days (Fig. 6c,d) shows that the width of the nanorings is 300nm and the shows several micrometer in diameter. Thickness of the nanoribbons were found to be in the range of 100-250nm. SAED pattern (Fig. 6f) taken on the nanoribbons of the sample corresponds to $Na_{0.3}V_2O_5$. Above observation clearly shows that the rings are made up of nanoribbons or nanorods or nanowires.

3.2 Electrochemical performance of V_2O_5 nanorings/nanoribbons

Cyclic voltammetry (CV) experiments were conducted to evaluate the electrochemical performance of V_2O_5 nanorings/nanoribbons at a scanning rate of 0.5 mVs^{-1} over the voltage range 1.5 – 4 V. Fig. 7 shows the cyclic voltammograms of the product prepared at various conditions. Well-defined reduction (cathodic) and oxidation (anodic) peaks occur at 2.4 V

(lithiation) and 2.8 V (delithiation) respectively, for the V_2O_5 nanorings/nanobets. The reversible chemical intercalation and deintercalation reaction [36,37] can be described as

$$\alpha - V_2O_5 + 0.5Li^{+1} + 0.5e^- \leftrightarrow \xi - Li_{0.5}V_2O_5 \qquad (1)$$

$$\xi - Li_{0.5}V_2O_5 + 0.5Li^{+1} + 0.5e^- \leftrightarrow \delta - LiV_2O_5 \qquad (2)$$

The capacity and cycle performance of V_2O_5 nanorings/nanoribbons electrodes are evaluated by galvanostatic discharge–charge measurements (Fig. 8) at a current density of 100 mA g^{-1}. The V_2O_5 nanorings/nanoribbons prepared at 130 °C for 1 day shows an initial discharge capacity of 275 mAh g^{-1}, and the capacity gradually decreases in the further cycles but remained at 200 mAhg^{-1} (27% capacity loss) after the 30th cycle (Fig. 8a). The initial high capacity of the nanorings/ribbons can be ascribed to the large surface area and short diffusion distances provided by the nanostructure. V_2O_5 nanorings/nanoribbons shows a surface area of 102 m^2/g is expected to present good rate capability and cyclability as the anode material in a Li-ion battery. Fig. S7 shows the discharge profiles exhibit one plateau which is consistent with the cyclic voltammogram. Fig. S8 shows the SEM images of the cathode materials after charge-discharge performances. It shows that there is a destruction of the structure and the product is agglomerated. Fig. 9 and Fig. S9 shows the cycling performances and charge-discharge profiles of V_2O_5 nanorings/nanoribbons at different current densities.

3.3 Formation mechanism

V_2O_5 nanorings are formed in aqueous solutions. Therefore, they should result from the condensation of molecular precursors. A whole range of molecular species can be observed in aqueous solutions at room temperature depending on pH and concentration. Around pH≈ 8, $NaVO_3$ are built of corner-sharing four-fold coordinated [VO_4] tetrahedra. Co-ordination

11

expansion occurs upon the acidification of aqueous solutions leading to vanadic species in which V^{5+} ions are in $[VO_5]$ square pyramids. The aqueous solution then turns from colorless to red. In dilute solutions, the neutral precursor $[VO(OH)_3(OH_2)_2]^0$ is obtained around pH$\approx$2. Deprotonation occurs at higher pH leading to $[VO(OH)_4(OH_2)]^-$ species around pH$\approx$6.

It is well known that the acidification of aqueous metavanadate solutions leads to the formation of $V_2O_5 \cdot nH_2O$ gels [2]. These are formed of ribbon-like V_2O_5 particles about 1 µm long, 20 nm wide and 2 nm thick. Because of the high polarizing power of small V^{5+} ions, surface V-OH groups exhibit acidic properties so that V_2O_5 gels could also be described as poyvanadic acids $H_nV_2O_5$ (n$\approx$ 0.3). Acidic protons can be easily exchanged with alkaline cations leading to $M_{0.3}V_2O_5 \cdot nH_2O$ (M = Li, Na, …) intercalated compounds.

The acidification of metavanadate solutions can be conveniently performed via an ion exchange between Na^+ and H^+ in a resin leading to the formation of $V_2O_5 \cdot nH_2O$. Na^+ ions are not removed when acidification is performed by adding an acid, they remain intercalated within the layered oxide leading to a poorly crystallized $Na_{0.3}V_2O_5,1.5H_2O$. Moreover, the presence of foreign cations introduces new electrostatic interactions leading to floculation rather than gelation [18]. Two phases can actually be formed upon acidification of sodium metavanadate aqueous solutions namely $Na_{0.3}V_2O_5 \cdot nH_2O$ ribbons and a layered $NaV_3O_8 \cdot 1.5H_2O$. Their respective amounts depend on experimental conditions, pH, temperature, ageing, etc. The hydrated trivanadate is formed above pH 5 while a mixture of $Na_{0.3}V_2O_5,1.5H_2O$ and $NaV_3O_8,1.5H_2O$ is observed in the pH range 3-5 [18]. These solid phases are formed via the condensation of hydroxyl V-OH groups in the equatorial 'xy' plane. Olation and oxolation reactions of the neutral precursor $[VO(OH)_3(OH_2)_2]^0$ around pH$\approx$2 lead to the 1-D ribbon-like particles of $V_2O_5 \cdot nH_2O$ gels whereas only oxolation reactions occur with $[VO(OH)_4(OH_2)]^-$ at a

neutral pH leading to 2-D structures. The hydrated trivanadate results from the co-condensation of both molecular precursors, $[VO(OH)_3(OH_2)_2]^0$ and $[VO(OH)_4(OH_2)]^-$ leading to the formation of trivanadate $[V_3O_8]^-$ layers with intercalated Na^+ in order to compensate the negative charge of the layers. Upon hydrothermal conditions, electrostatic interactions between the V_2O_5 layers decrease, leading to the progressive deintercalation/ extraction of Na^+ cations from the $Na_{0.3}V_2O_5 \cdot nH_2O$ phase. The self-rolling of flexible exfoliated V_2O_5 nanoribbons can then occur. A similar process has already been suggested for the synthesis of TiO_2 nanotubes via the exfoliation of layered titanate $Na_2Ti_3O_7$ [38] or niobium oxide from $K_4Nb_6O_{17}$[39].

The self-coiling of a single nanobelt mechanism has been suggested to explain the formation of ZnO nanorings [27]. Because of their polar surface, flexible ZnO nanoribbons roll over into nanorings in order to reduce the electrostatic energy. $[VO_5]$ square pyramids also exhibit a polar structure with a short V=O opposite to a long V---OH_2 bond along the 'z' axis (O=V---OH_2). The α- V_2O_5 is made of chains of edge sharing $[VO_5]$ square pyramids in which V=O are directed towards opposite directions in two adjacent pyramids. The whole structure is therefore non polar. This is no longer the case for VO_x nanotubes in which the oxide layers are built of two sheets of $[VO_5]$ square pyramids pointing in opposite directions and are linked by $[VO_4]$ tetrahedral [40]. Again the whole structure is non-polar, but each $[VO_5]$ sheet has a polar structure. VO_x nanotubes are formed under hydrothermal conditions at a higher pH allowing the formation of tetrahedral $[VO_4]$ species. In our case, the pH of the precursor solution is too low for tetrahedral co-ordination to occur. V_2O_5 nanoloops are made of single sheets of $[VO_5]$ square pyramids only. Such sheets can exhibit a polar structure. The self-rolling process could involve nanoribbons and nanoribbons rather than nanosheets leading to nanorings rather than nanotubes.

The possible growth mechanism for the formation of $Na_{0.3}V_2O_5$ nanofibers and V_2O_5 nanorings are shown in the schematic diagram 1.

4. Conclusion

In conclusion, we have reported the hydrothermal synthesis of V_2O_5 nanorings and $Na_{0.3}V_2O_5$ nanoribbons without using any surfactant in aqueous acidic medium. Electrochemical tests indicated that the V_2O_5 nanorings/nanoribbons has an initial specific capacity of 280 mAh g^{-1} in the 1.5-4 V vs. Li^+/Li, and its stabilized capacity still remained as high as 200 mAh g^{-1}. The formation mechanism of nanorings and nanoribbons involve a simple ion intercalation/ deintercalation process. The self-rolling process of polar [VO_5] square pyramids involves nanoribbons and nanoribbons lead to the formation of nanorings. These nanorings exhibit a well ordered crystalline structure of α- V_2O_5. Further studies on the improvement in the quantity/ quality of V_2O_5 nanorings and the generation of other metal oxide nanorings are under research.

References

[1] M.S. Whittinham, J. Electrochem. Soc. 123 (1976) 315.

[2] J. Livage, Chem. Mater. 3 (1991) 578.

[3] A. Pan, J.G. Zhang, Z. Nie, G. Cao, B.W. Arey, G. Li, S.Q. Liang, J. Liu, J. Mater. Chem. 20 (2010) 9193.

[4] L. Mai, L. Xu, C. Han, X. Xu, Y. Luo, S. Zhao, Y. Zhao, Nano Lett. 10 (2010) 4750.

[5] A.M. Cao, J.S. Hu, H.P. Liang, L.J. Wan, Angew. Chem. Int. Ed. 44 (2005) 4391.

[6] J. Liu, H. Xia, D. Xue, L. Lu, J. Am. Chem. Soc. 131 (2009) 12086.

[7] M. Ponzi, C. Duschatzky, A. Carrascull, E. Ponzi, Appl. Catal. A, 373 (1998) 373.

[8] A.L. Lemonidou, M. Machli, Catal. Today 127 (2007) 132.

[9] K. Takahashi, Y. Wang, G.Z. Cao, Appl. Phys. Lett. 86 (2005) 053102.

[10] I.H. Kim, J.H. Kim, B.W. Cho, Y.H. Lee, K.B. Kim, J. Electrochem. Soc. A. 153 (2006) 989.

[11] G. Gu, M. Schmid, P.W. Chiu, A. Minett, J. Fraysse, G.T. Kim, S. Roth, M. Kozlov, E. Munoz, R. H. Baughman, Nat. Mater. 2 (2003) 316.

[12] C.M. Leroy, M.F. Achard, O. Babot, N. Steunou, P. Masse, J. Livage, L. Binet, N. Brun, R. Backov, Chem. Mater. 19 (2007) 3988.

[13] D. Yu, C. Chen, S. Xie, Y. Liu, K. Park, X. Zhou, Q. Zhang, J. Li, G. Cao, Energy Environ. Sci. 4 (2011) 858.

[14] F. Coustier, J. Hill, B.B. Owens, S. Passerini, W.H. Smyrl, J. Electrochem. Soc. 146 (1999) 1355.

[15] J.X. Wang, D.L. Schulz, J.G. Zhang, J. Electrochem. Soc. 151 (2004) A1.

[16] D.W. Kim, Y.D. Ko, J.G. Park, B.K. Kim, Angew. Chem. Int. Edn. 46 (2007) 6654.

[17] M. Pasquali, G. Pistoia, Electrochim. Acta 36 (1991) 1549.

[18] O. Durupthy, N. Steunou, T. Coradin, J. Maquet, C. Bonhomme, J. Livage. J. Mater. Chem. 15 (2005) 1090.

[19] Y. Chen, X. Li, X.Y. Zhou, H. Yao, H. Huang, Y.W. Maiad and L. Zhou, Energy Environ. Sci., 7 (2014) 2689

[20] J.C. Hulteen, C.R. Martin, J. Mater. Chem. 7 (1997) 1075.

[21] B.B. Lakshmi, C.J. Patrissi, C.R. Martin, Chem. Mater. 9 (1997) 2544.

[22] Y. Chen, Z. Li and X.W. Lou, Angew. Chem. Int. Ed. 54 (2015) 10521

[23] K. Takahashi, S.J. Limmer, Y. Wang, G.J. Cao, J. Phys. Chem. B. 108 (2004) 9795.

[24] Y. Chen, X. Li, K. Park, J. Song, J. Hong, L. Zhou, Y.W. Mai, H. Huang and J. B. Goodenough, J. Am. Chem. Soc. 135 (2013)16280

[25] Q. Su, C.K. Huang, Y. Wang, Y.C. Fan, B.A. Lu, W. Lan, Y.Y. Wang, X.Q. Liu, J. Alloys and Compounds 475 (2009) 518.

[26] J. Livage, Materials 3 (2010) 4175.

[27] X.Y. Kong, Y. Ding, R.S. Yang, Z. L. Wang, Science 303 (2004) 1348.

[28] G. Shen, D. Chen, J. Am. Chem. Soc. 128 (2006) 11762.

[29] R.S. Yang, Z.L. Wang, J. Am. Chem. Soc. 128 (2006) 1466.

[30] F. Zhu, Z.X. Yang, W.M. Zhou, Y.F. Zhang, Phys. Stat. Sol. (a). 203 (2006) 2024.

[31] X. Wang, G. Xi, S. Xiong, Y. Liu, B. Xi, W. Yu, Y. Qian, Crystal Growth & Design 7 (2007) 930.

[32] J. Liu, D. Xue, Nanoscale Res Lett. 5 (2010) 1619.

[33] G.T. Chandrappa, P. Chithaiah, S. Ashoka, J. Livage, Inorg. Chem 50 (2011) 7421.

[34] S. Ashoka, G. Nagaraju, K.V. Thipperudraiah, G.T. Chandrappa, Mater. Research Bulletin 45 (2010) 1736.

[35] F. Li, X. Wang, C. Shao, R. Tan, Y. Liu, Mater. Lett. 61 (2007) 1328.

17

[36] J.S. Sakamoto, B. Dunn, J. Electrochem. Soc. 149 (2002) A26.

[37] S.H. Ng, T.J. Patey, R. Buchel, F. Krumeich, J.Z. Wang, H.K. Liu, S.E. Pratsinis, P. Novak, Phys. Chem. Chem. Phys. 11 (2009) 3748.

[38] M. Wei, Y. Konishi, H. Zhou, H. Arakawa, Solid State Comm. 133 (2005) 493.

[39] Y. Kobayashi, H. Hata, M. Salama, T.E. Mallouk, Nano Lett. 7 (2007) 2142.

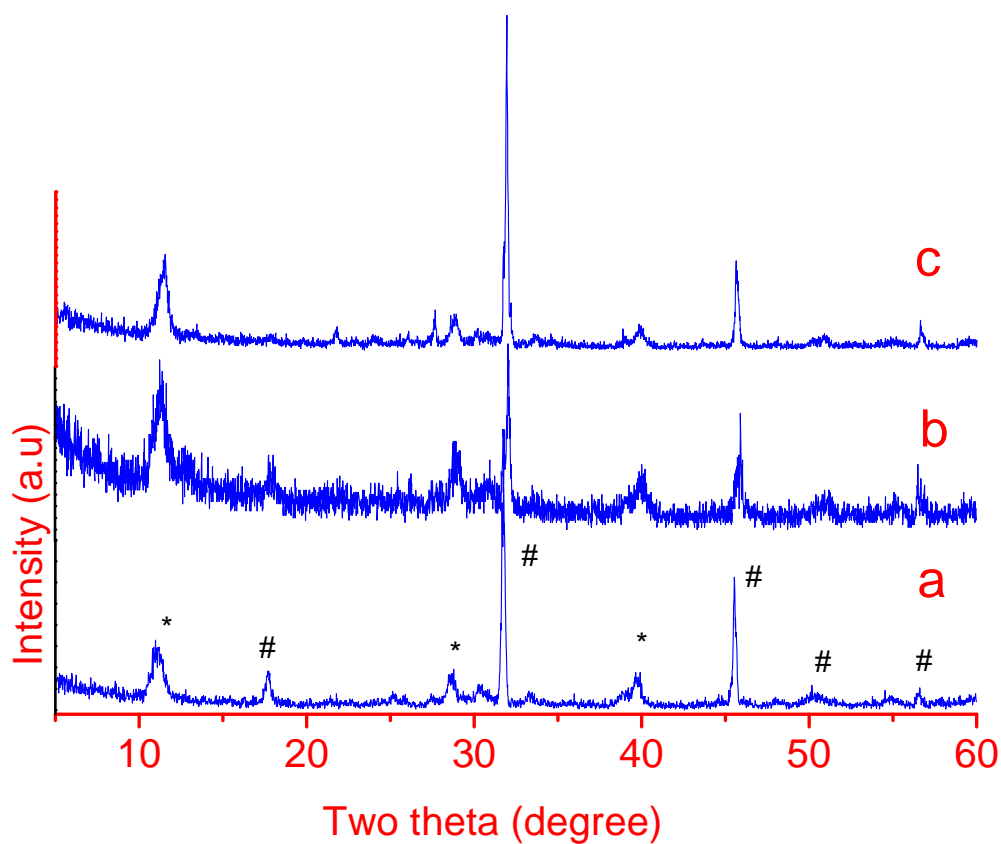[40] M. Wörle, F. Krumeich, F. Bieri, H-J. Muhr, R. Nesper, Z. Anorg. Allg. Chem. 628 (2002) 2778.

Fig. 1. PXRD patterns of the nanorings/nanoribbons prepared at **(a)** 130 °C for 2 days, (b) 150 °C for 2 days and (c) 110 °C for 3 days. (* = $Na_{0.3}V_2O_5$, # = V_2O_5)
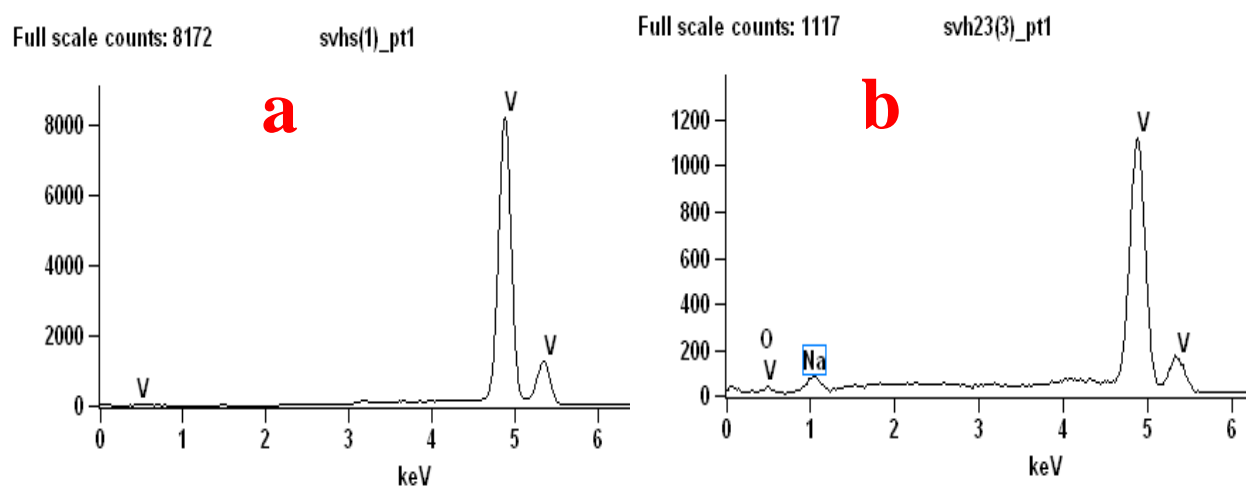
Fig. 2 EDS spectrum of (a) nanorings and (b) nanoribbons prepared at 130 °C for 2 days.
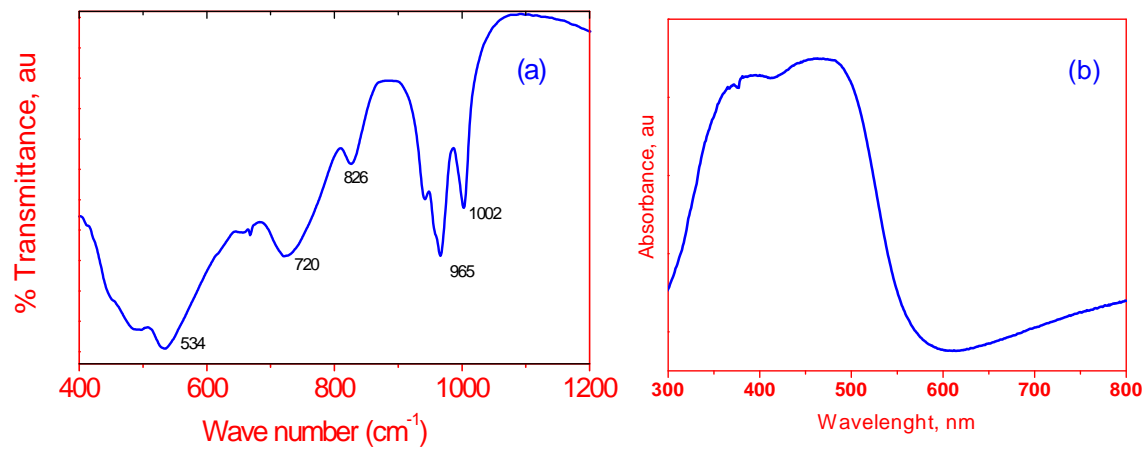
Fig. 3. (a) FTIR spectrum and (b) UV-Vis spectrum of the V_2O_5 nanorings/ nanoribbons prepared at 130 ℃ for 2 days.
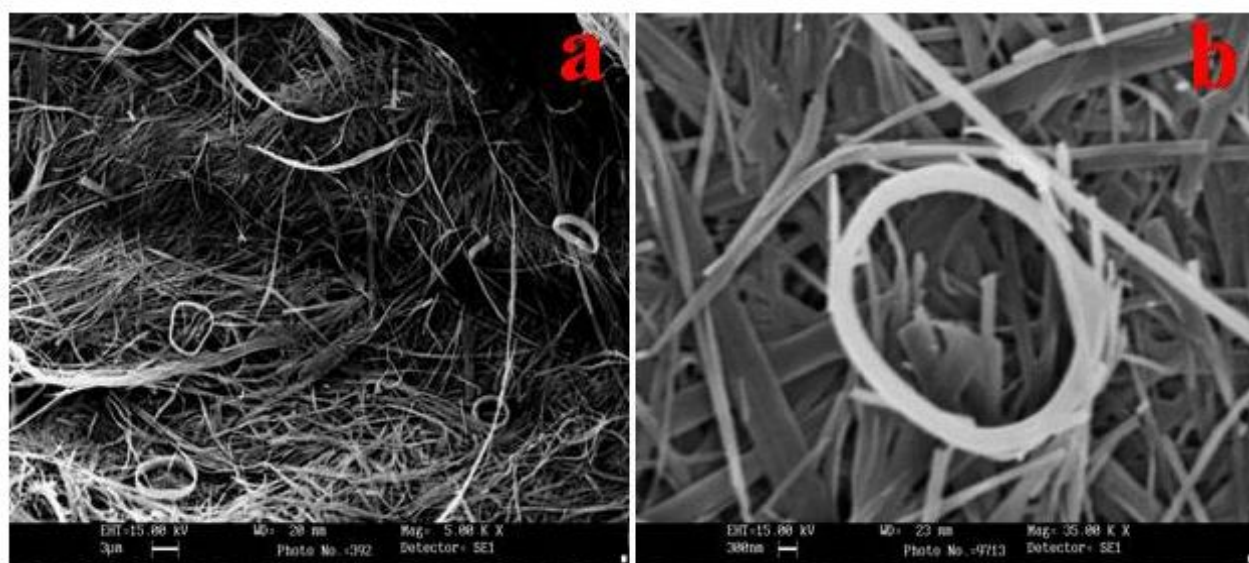
Fig. 4 SEM images of the nanorings/nanoribbons prepared at (a) 100 °C and (b) 110 °C   for 3 days.
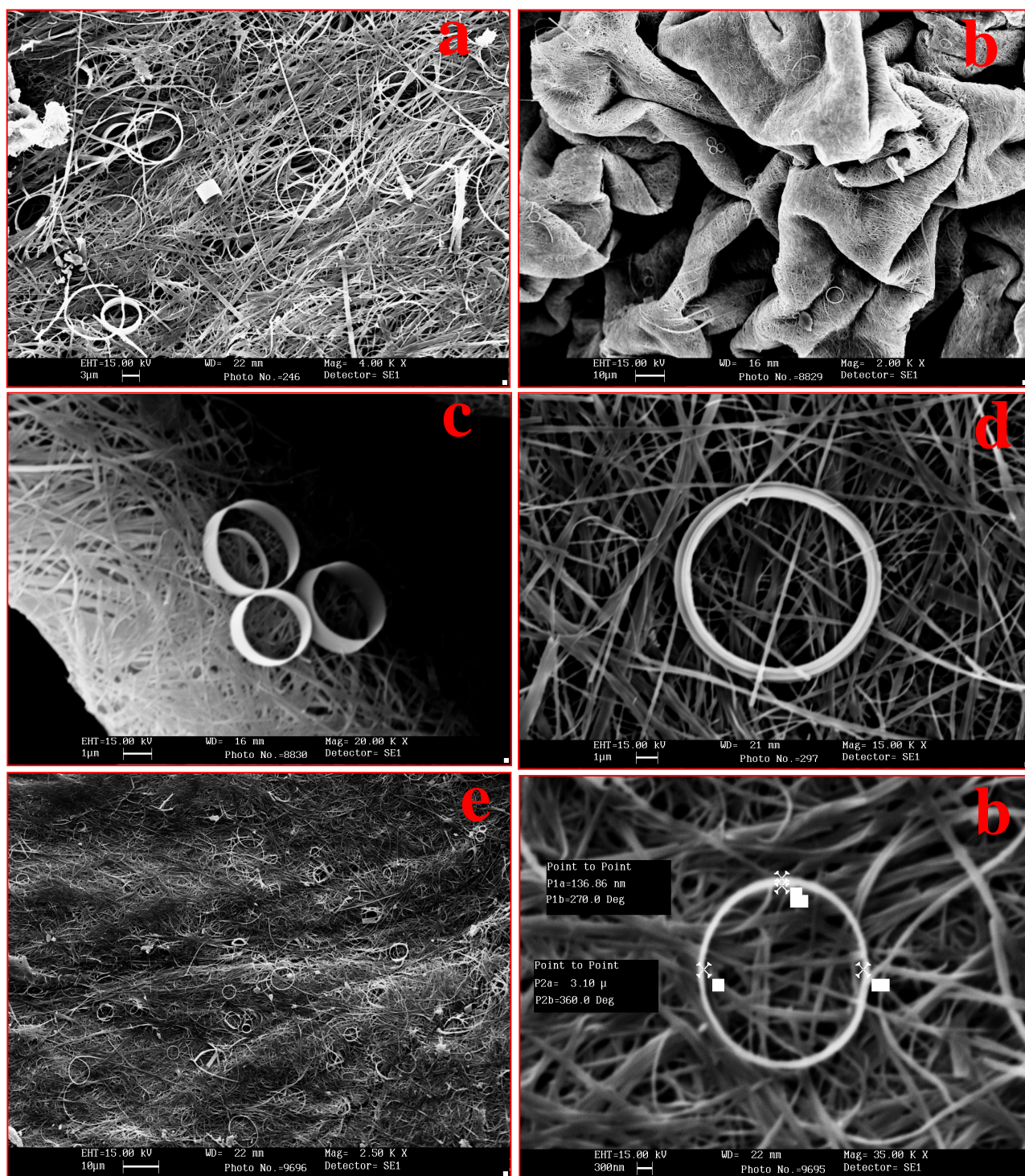
21

Fig. 5. SEM images of the nanorings/nanoribbons prepared at (a) 130 °C for 1 day, (b,c)130 °C for 2 days, (d) 150 °C for 1 day and (e,f) 150 °C for 2 days.
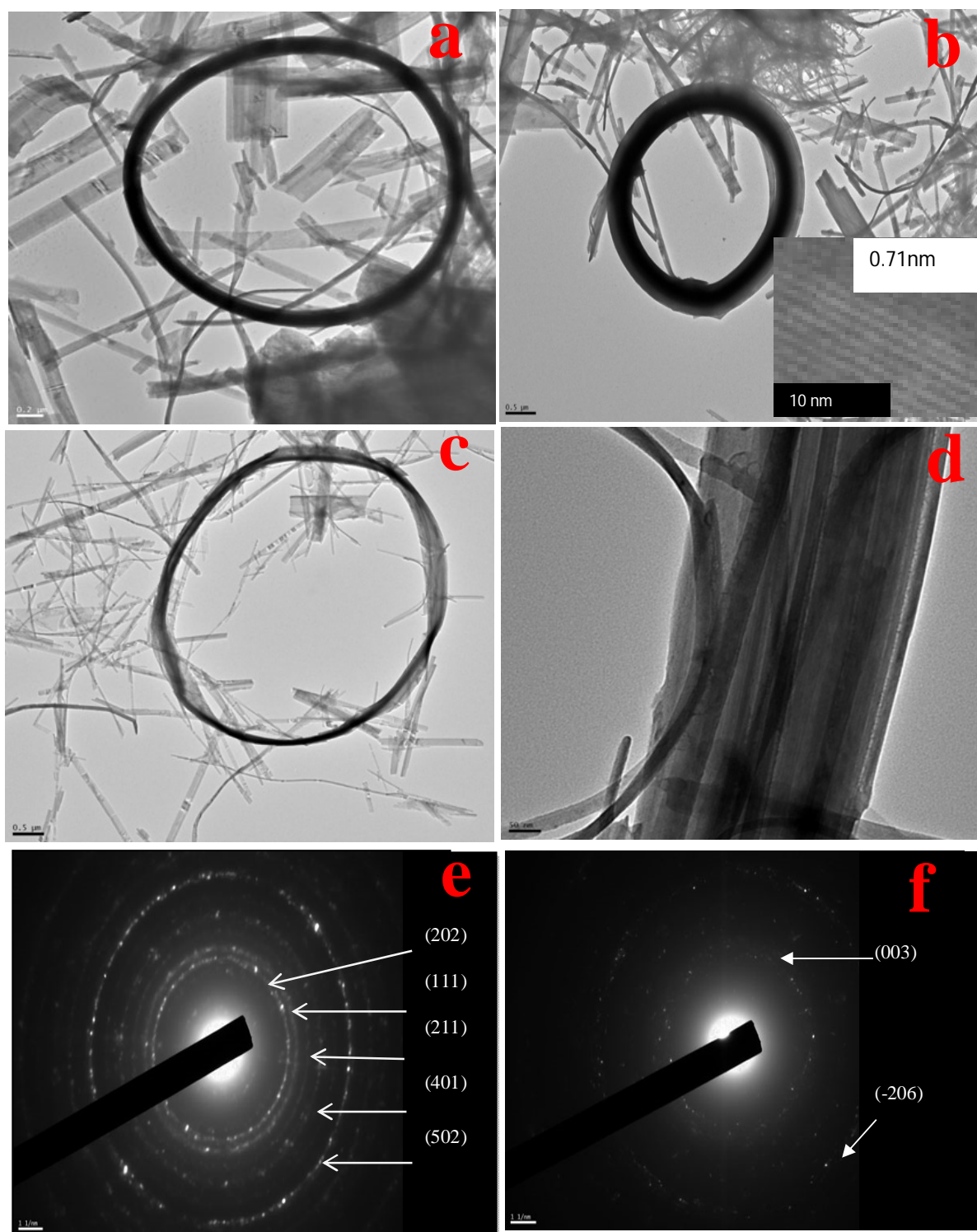
Fig. 6 TEM image of (a,b) nanorings/nanoribbons, (inset- HRTEM of nanorings) prepared at 110 °C for 3 days, (c,d) nanorings/nanoribbons prepared at 150 °C for 2 days and SAED patterns of (e) nanorings and (f) nanoribbons prepared at 110 °C for 3 days.
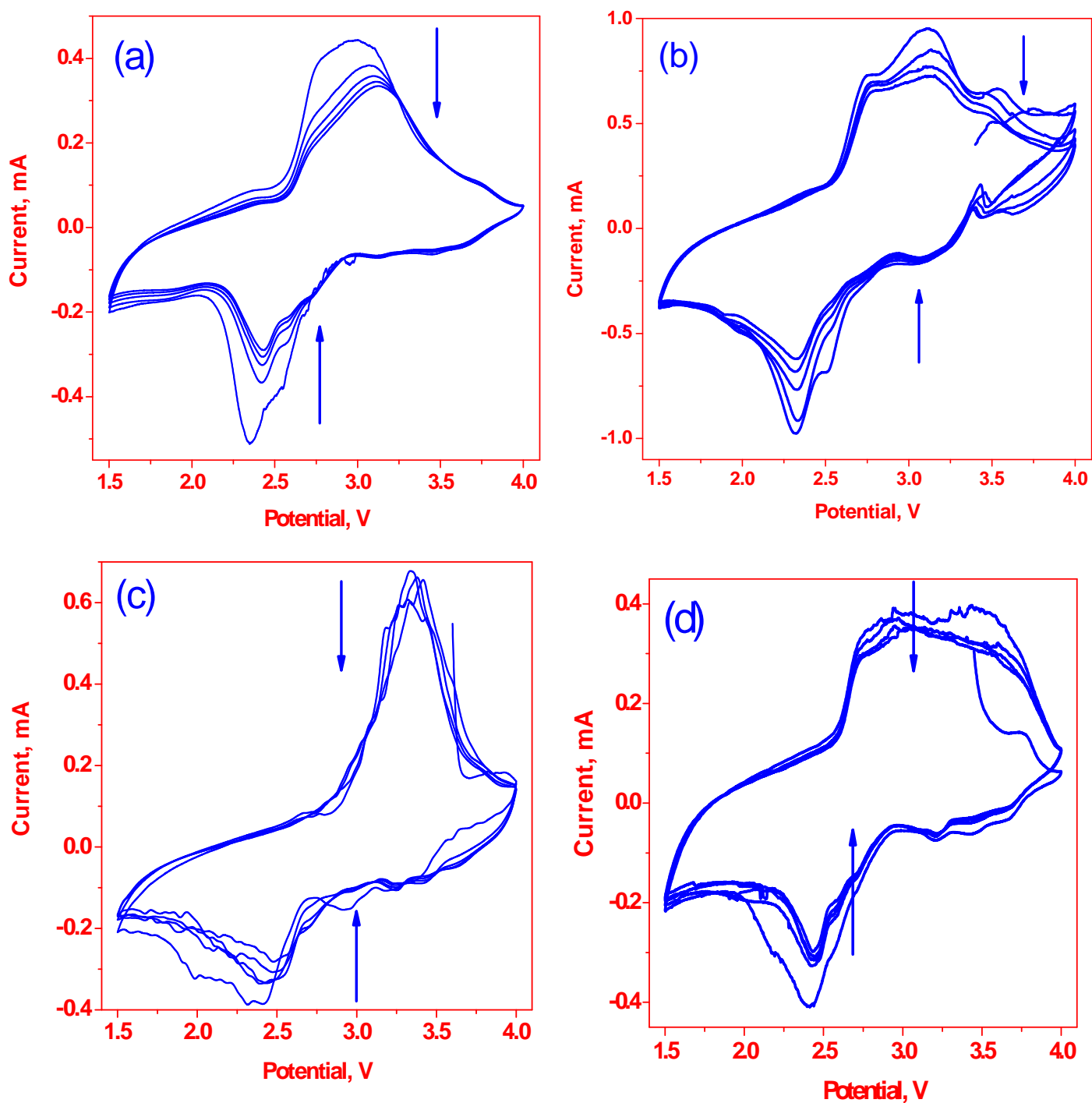
Fig. 7. Cyclic voltammograms of the V_2O_5 nanorings/nanoribbons prepared at (a) 130 ° C for 1 day, (b) 130 ° C for 2 days, (c) 150 ° C for 1 day and (d) 150 ° C for 2 days at a scan rate of 0.5 mVs^{-1} between 1.5-4 V.
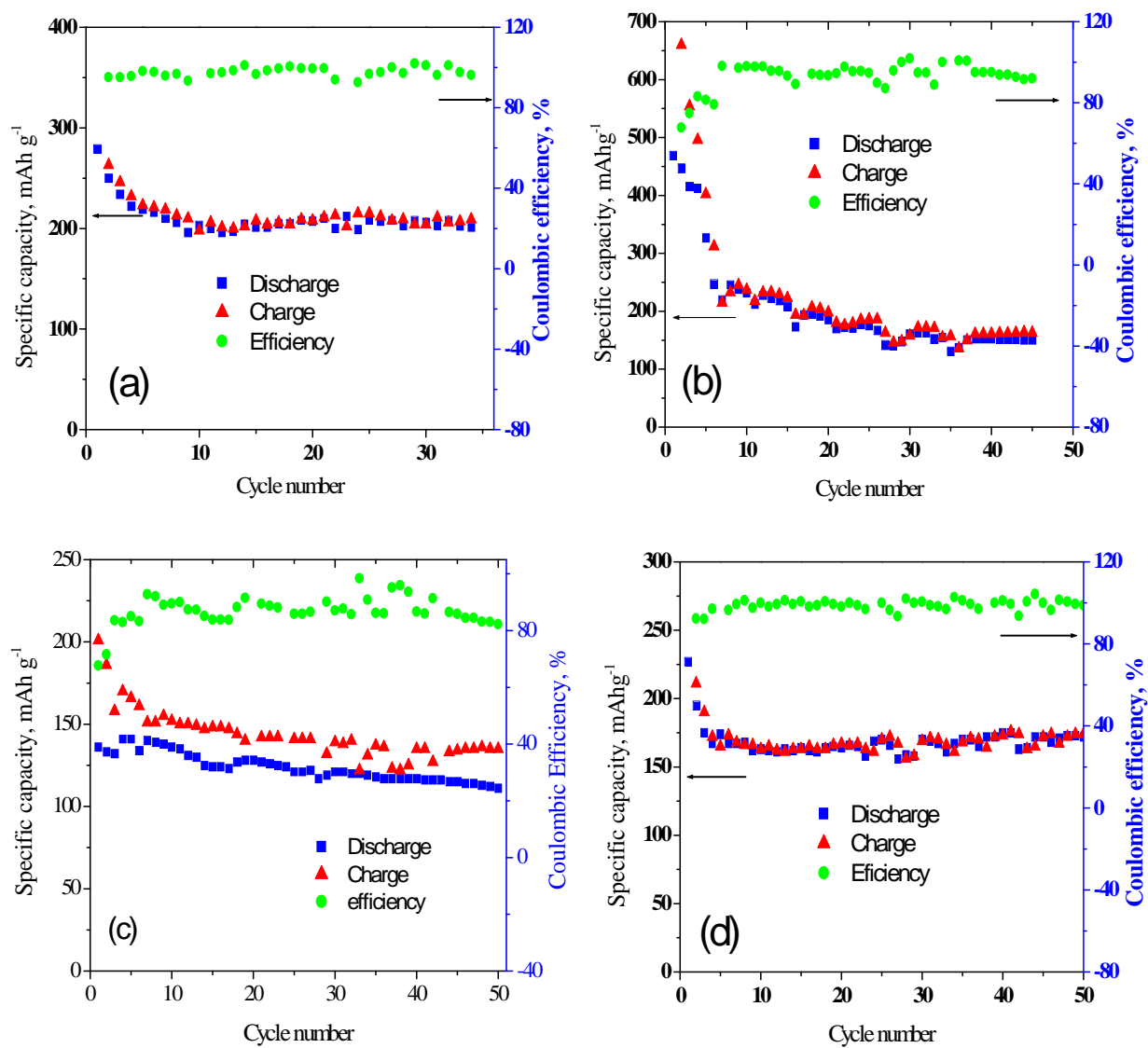
Fig. 8. Cycling performance (discharge and charge capacity), Coulombic efficiency of the V_2O_5 nanorings /nanoribbons prepared at (a) 130 º C for 1 day, (b) 130 º C for 2 days, (c) 150 º C for 1 day and (d) 150 º C for 2 days at a current density of 0.1 mA g^{-1}.
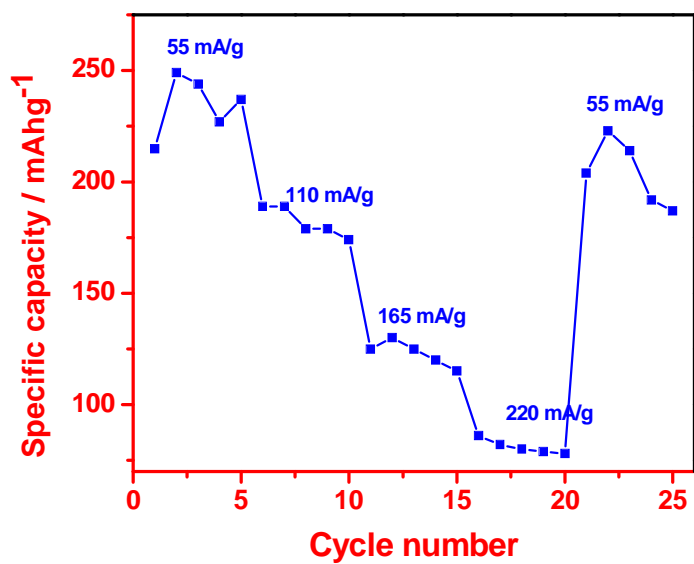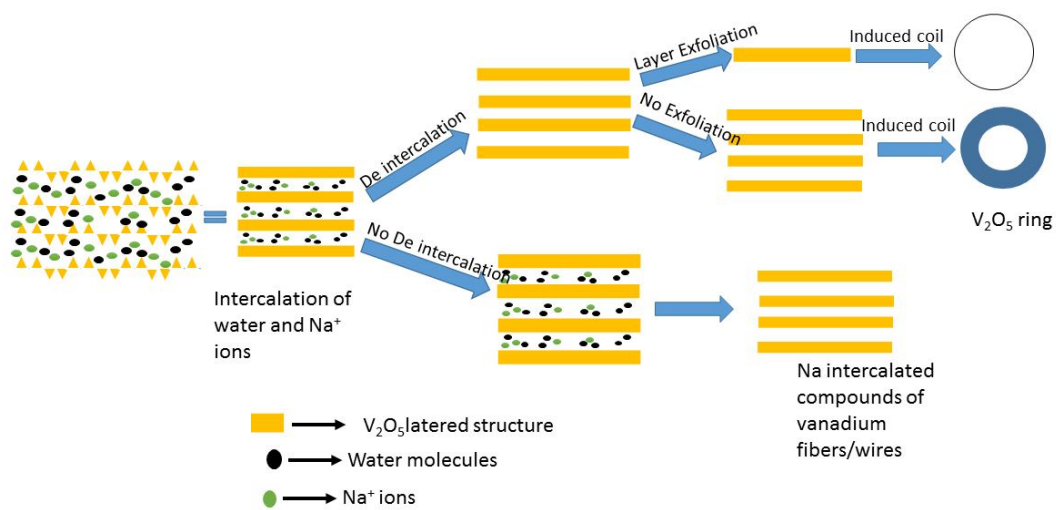
Fig. 9. Discharge and charge profile of V_2O_5 nanorings/nanoribbons prepared at 130 º C for 2 day at a different current densities of 55 mA/g for 1-5 cycles, 110 mA/gfor 6-10 cycles, 165 mA/g for 11-15 cycles, 220 mA/g for (16-20 cycles and 55 mA/g for 21-26 cycles,

26

Scheme 1. Possible schematic growth diagram of $Na_{0.3}V_2O_5$ nanofibers/ nanorings.